Acta Oceanol. Sin., 2020, Vol. 39, No. 8, P. 88–95
https://doi.org/10.1007/s13131-020-1637-6
http://www.hyxb.org.cn
E-mail: hyxbe@263.net

The pressure compensation technology of deep-sea sampling based on the real gas state equation

Shuo Wang[1, 2], Shijun Wu[1]*, Canjun Yang[1]

[1] State Key Laboratory of Fluid Power and Mechatronic Systems, Zhejiang University, Hangzhou 310027, China

[2] Institute of Deep-Sea Science and Engineering, Chinese Academy of Sciences, Sanya 572000, China

Received 12 July 2019; accepted 18 December 2019

Abstract

Compressed gas is usually used for the pressure compensation of the deep-sea pressure-maintaining sampler. The pressure and volume of the recovered fluid sample are highly related to the precharged gas. To better understand the behavior of the gas under high pressure, we present a new real gas state equation based on the compression factor Z which was derived from experimental data. Then theoretical calculation method of the pressure and volume of the sample was introduced based on this empirical gas state equation. Finally, the proposed calculation method was well verified by the high-pressure vessel experiment of the sampler under 115 MPa.

Key words: gas state equation, deep-sea sampler, pressure compensation, sample pressure, sample volume

Citation: Wang Shuo, Wu Shijun, Yang Canjun. 2020. The pressure compensation technology of deep-sea sampling based on the real gas state equation. Acta Oceanologica Sinica, 39(8): 88–95, doi: 10.1007/s13131-020-1637-6

1 Introduction

The deep sea is the largest habitat on earth, with at least 50% of the total biosphere lying below a depth of 1 000 m in the ocean. Our knowledge of deep-sea ecosystems remains very limited compared to that for continental shelf ecosystems (Drazen and Yeh, 2012). This extreme environment is characterized by the absence of light, low temperature, and high hydrostatic pressure (Koyama et al., 2002; Pavithran et al., 2007). A variety of topographical features exist in deep-sea environments, such as hydrothermal vents, cold seeps, oceanic trenches, seamounts, and bathyal plains, which possess different physical and chemical properties (Zhang et al., 2018). Extremophiles could be sensitive to drastic changes in pressure and temperature and may be sensitive to changes in atmospheric pressure (Kim and Kato, 2010). Studies on microbes in extreme environments can deepen the understanding of deep-sea microbes' survival principles and deep-sea microbes' functions in the food chain (Huang et al., 2006). Humans currently do not understand the ecology and biology of the deep-sea biota because this remote environment is difficult and expensive to access and sample (Shillito et al., 2015). There are numerous methods to obtain samples from the deep sea, such as trawls, water samplers, microbe samplers, multi-bottle rosette samplers, bellows type samplers, box-core sediment samplers and grab samplers equipped with a camera (Koyama et al., 2002; Kim and Kato, 2010; Bianchi et al., 1999). Researchers have enabled investigations of seabed sulfides by developing near-bottom vehicles, including autonomous underwater vehicles (AUV), human-occupied vehicles (HOV), and remote-operated vehicles (ROV) (Wu et al., 2019).

Maintaining the *in-situ* pressure of a sample can prevent the chemical and biological properties of the sample from changing due to the release of dissolved volatile components caused by decompression (Huang et al., 2018; Rossel et al., 2017). International researchers have developed a variety of high-pressure instruments to collect samples at depth and to retrieve them to the surface under pressure, including isobaric fluid samplers, sediment samplers, pressure-stat aquarium systems, high-pressure fish trap-respirometers and the AbyssBox for permanent public exhibitions of live deep-sea hydrothermal fauna (Koyama et al., 2002; Shillito et al., 2015; Wu et al., 2010; Yamamoto, 2015; Drazen et al., 2005; McNichol et al., 2016; Peoples et al., 2019). These high-pressure sampling instruments are an inseparable part of pressure compensation technologies. The scientific community is willing to use sampling instruments with pressure-maintaining functions if the technology permits.

For a deep-sea sampler, an accumulator with compressed gas is usually used to compensate the pressure loss that is caused by small volume changes due to leakage, cubic deformation of the vessel and the compression of sealing materials (Huang et al., 2006; Jannasch and Wirsen, 1977). Previously, the parameters of the pressure compensation technique, such as the sample volume and sample pressure, were usually calculated by using the ideal gas state equation. Although most existing real gas state equations have quite good accuracy at pressures below 30 MPa, the calculation errors for these parameters increases as the pressure increases (as shown in Fig. 1), which makes them ill-suited for the samplers used for abyssal and hadal zones (Wu et al., 2018).

This paper presents an empirical real gas state equation and theoretical calculation method for deep-sea sampling equipment. The degree of deviation for some existing real gas state equations in ultrahigh pressures was analyzed and compared. The gas compression experiments were conducted according to the deep-sea gas pressure compensation range. We next proposed a simple gas state equation for pressures ranging from 15

Foundation item: The National Key Research and Development Program of China under contract Nos 2018YFC0310600 and 2016YFC0300500.

*Corresponding author, E-mail: bluewater@zju.edu.cn

to 120 MPa by fitting the data from the experiments. A theoretical calculation method for the sample volume and sample pressure of the sampler was proposed by combining with the real gas state equation. Finally, the calculation method was well verified by a high-pressure vessel experiment for the sampler under 115 MPa.

2 Comparison of the gas state equations

The state of a certain amount of pure gas can be determined when two of P, V and T are given. This functional equation is called an equation of state (EOS), namely, $f(P, V, T)=0$ (Smith et al., 2005). The simplest realistic model equation of state is the ideal gas equation of state, which is acceptable at low pressures. Under high pressure, an actual gas is increasingly resistant to compression as the molecules move closer together (Priede, 2018). To represent the PVT behavior of both liquids and vapors, it is essential to obtain an equation of state that encompasses a wide range of temperatures and pressures with no limitation (Halder, 2014). In this regard, numerous such equations have been proposed (Hempert et al., 2017). The compression factor, Z, which accounts for the deviation from ideal gas behavior, is defined by $Z=PV/RT$ (also known as the Virial Equation), where $Z=1$ for an ideal gas (Monago, 2010). The PVT relations of real gases have been elaborately discussed, with some better-known equations involving large-scales of pressures and temperatures, such as the van der Waals (vdW), Peng-Robinson (PR), Redlich-Kwong (RK), Soave-Redlich-Kwong (SRK), and Martin-Hou (MH) equations of state (Redlich and Kwong, 1949; Martin and Hou, 1955; Soave, 1972; Peng and Robinson, 1976). Descriptions of these EOSs are shown in Table 1. These types of equations are complicated in form but are very capable of providing accurate results. Therefore, these equations are successfully and widely used in different areas.

Table 1. Different EOS types for real gases

Type	Real gas EOS
vdW	$P=\frac{RT}{V-b}-\frac{a}{V^2}$
Virial	$Z=\frac{PV}{RT}=1+B'P+C'P^2+D'P^3+\cdots$
RK	$P=\frac{RT}{V-b}-\frac{a/\sqrt{T}}{V(V+b)}$
MH	$P=\sum_{i=1}^{5}\frac{f_i(T)}{(V-b)^i}$
SRK	$P=\frac{RT}{V-b}-\frac{\alpha(T)}{V(V+b)}$
PR	$P=\frac{RT}{V-b}-\frac{a}{V(V+b)+b(V-b)}$

To examine whether the existing real gas state equations are well-suited for full ocean depths, a gas compression experiment ranging from 15 to 120 MPa was designed according to the deep-sea gas pressure compensation range. More details of the experiment are introduced in Section 3.2. Experimental data were accounted for in existing real gas state equations to calculate theoretical gas pressure values. The relative errors of the theoretical values were obtained by comparing them with the experimental pressure values (as shown in Fig. 1).

Most existing real gas state equations have small errors at pressures ranging from 15 to 30 MPa, but these deviations increase gradually as the pressure increases. Therefore, an appropriate gas state equation should be chosen to deal with high pressures of up to 120 MPa and should calculate the deep-sea sampler parameters conveniently and precisely.

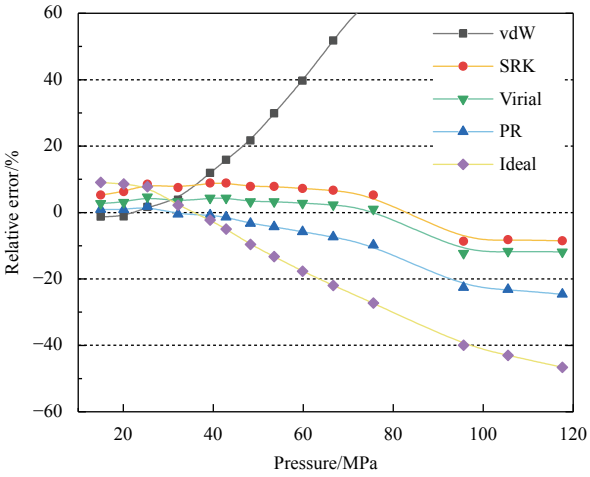

Fig. 1. The relative error between the theoretical and real pressure values calculated by different gas state equations.

3 Real gas state equation based on compressibility factor

3.1 *The real gas state equation for high pressure*

This paper presents an empirical gas state equation that is used for deep sea sampling techniques. It is shown as Eq. (1).

$$Z(P)=\frac{PV}{nRT}=a_1P^2+a_2P+a_3, \tag{1}$$

where $a_1=1.416\,3\times10^{-5}$, $a_2=8.619\,4\times10^{-3}$, and $a_3=0.804\,9$ when 15 MPa$\leqslant P\leqslant$120 MPa. Z is the compression factor, P is the pressure, V is the volume, n is the amount of material, R is a gas constant and T is the temperature.

3.2 *Gas compression experiment and calculation*

A gas compression experiment was designed to verify the feasibility of the existing gas state equations at pressures ranging from 15 to 120 MPa. The basic principle of the experiment is the variable controlling approach. For the three parameters of P, V and T, P is used as a variable and V and T are measured. As shown in Fig. 2, the experimental system is mainly composed of a high-pressure cylinder (with an inner diameter of 47 mm, a length of 115 mm), a water pump, and some stop valves, gauges and pipelines that can withstand pressures of up to 120 MPa. The high-pressure cylinder contains a piston and a baffle ring. The piston compresses the gas via a water pump, and the baffle ring ensures that the piston moves to a certain position. Pressure gauges I and II can detect the pressure of pure water and pure nitrogen at both sides of the piston. The water pump continuously injects pure water into the high-pressure cylinder to push the piston forward. The thermometer displays the temperature of the compressed gas in real time. The volume of the gas in the high-pressure cylinder at the beginning and end of the compression are 180.5 mL and 33 mL, respectively.

The main operations of the gas compression experiment include charging the gas to the cylinder and pressurizing the gas with the water pump. First, pure nitrogen gas is charged into the high-pressure cylinder by a gas pump. Then, the water pump continuously injects high-pressure water into the cylinder until the pressure of the gas no longer rises. The parameters of the gas are set to P_0, V_0 and T_0 when the gas is charged. The parameter

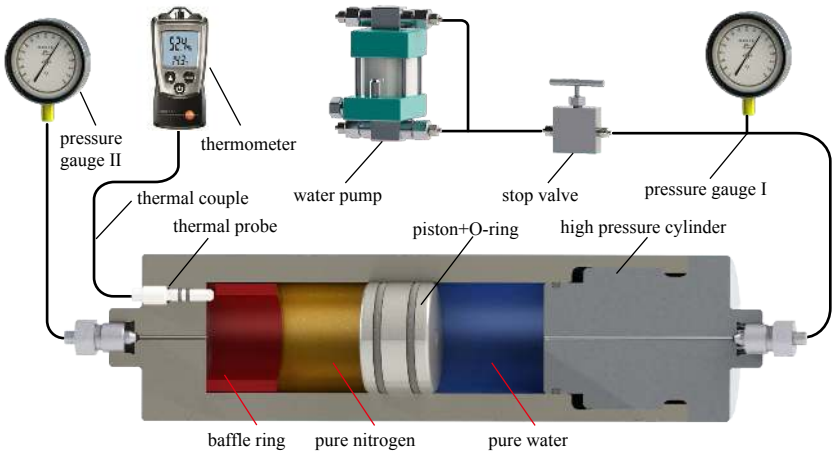

Fig. 2. Schematic diagram of the high-pressure system for the gas compression experiment.

values for the gas after the experiment are set to P_1, V_1 and T_1. Each group of experiments is repeated at least three times to ensure the accuracy of the results. The data of these experiments are shown in Table 2.

Table 2. The original values from the gas compression experiments

No.	P_0/MPa	P_1/MPa	V_0/mL	V_1/mL	T_0/K	T_1/K
1	2.96	15.86	180.50	33.03	293.8	294.7
2	3.58	19.47	180.50	33.03	294.9	295.4
3	4.02	22.33	180.50	33.03	295.0	295.4
4	5.10	30.15	180.50	33.03	294.2	295.3
5	6.04	38.52	180.50	33.03	294.2	295.2
6	6.95	48.54	180.50	33.03	294.8	295.6
7	8.01	62.84	180.50	33.03	294.7	295.4
8	8.93	78.82	180.50	33.03	294.5	295.7
9	9.26	86.31	180.50	33.03	294.5	297.4
10	9.97	101.28	180.50	33.03	297.7	298.9
11	10.32	110.21	180.50	33.03	296.2	296.5
12	10.48	114.21	180.50	33.03	296.5	297.3

3.3 *Calculation of fitting process*

The compression factor (Z) is defined in terms of the Ideal Gas Law:

$$Z = \frac{PV}{nRT}. \tag{2}$$

When the parameters such as pressure, volume and temperature are known, the value of Z can be solved, as long as the amount of substance "n" of the gas is solved. The "n" of the gas can be determined and will be constant during the compression process as long as the cylinder is precharged.

Since the precharge pressure is very low, we can choose a suitable existing gas equation to accurately calculate the parameters of the gas at the precharged stage. From Fig. 1, it can be seen that the relative error of PR is smaller than for other EOSs below 30 MPa. Therefore, the PR equation is chosen here (Peng and Robinson, 1976), which is shown in Eq. (3):

$$P = \frac{RT}{V-b} - \frac{a}{V(V+b)+b(V-b)}, \tag{3}$$

where $a = 0.457\,24\frac{R^2T_c^2}{P_c}\alpha(T)$ and $b = 0.077\,796\frac{RT_c}{P_c}$, $\alpha(T) = \left[1+\left(0.374\,64+1.542\,26\omega-0.269\,92\omega^2\right)\left(1-\sqrt{T/T_c}\right)\right]^2$, $R = 8.314$, $T_c = 126.2$ K, $P_c = 3.400\,000\,91$ MPa, and $\omega = 0.037\,72$.

The P_0, V_0, T_0 and other parameters of the precharged gas are substituted into the PR equation. When the value of V is solved, the value of "n" can be calculated according to the formula "$n = V_0/V$".

The values of P_1, V_1, T_1 and "n" after gas compression are brought into Eq. (2), and then the value of the gas compression factor "Z" can be determined. After the "Z" of each group of experiments is determined, the values of "Z" and pressure are plotted, as shown in Fig. 3. The data curve is fitted with MATLAB software to obtain the empirical equation of "Z" and "P", as shown in Eq. (1).

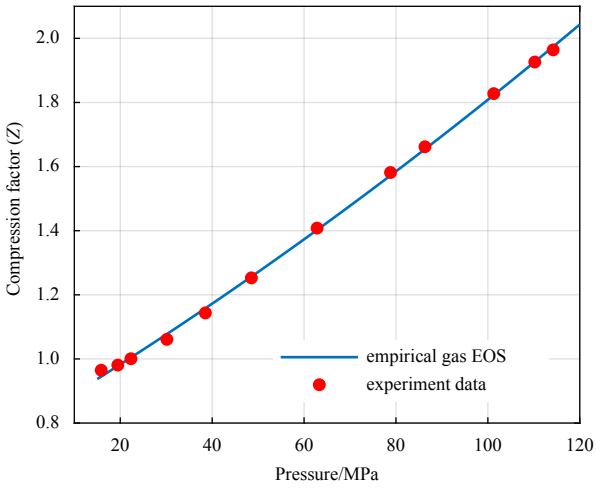

Fig. 3. Graphical representation of the compression factor versus pressure.

4 Pressure compensation of deep-sea sampler

4.1 *Description of the deep-sea pressure-maintaining fluid sampler*

The sampling cylinder is a part of the sampler that plays a vital role in collecting and maintaining the *in situ* pressure of the sample. It is composed of an accumulator chamber, a sample chamber, an orifice and two pistons (Fig. 4). The two pistons di-

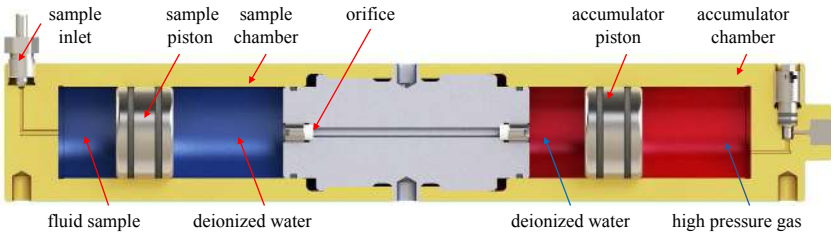

Fig. 4. Schematic diagram of the pressure-maintaining sampling cylinder.

vide the cylinder into three sections, which are filled with compressed gas, deionized water and the fluid sample. The compressed gas is used for pressure compensation and the orifice is used for controlling the flow velocity during the sampling process. This design of the sampling cylinder has previously been successfully applied in many field tests. At present, we are more concerned about the parameters of the sampling cylinder, such as the pressure of the precharged gas, the effect of pressure compensation and the sample volume. Prior to the theoretical calculations of these parameters, it is necessary to determine the actual operation of the sampling cylinder. There are three statuses of the cylinder during the whole process of sampling, as shown in Fig. 5.

Status I: When the sampler is being prepared on the deck, the accumulator chamber of the sampling cylinder is precharged with nitrogen at a pressure of approximately 10% to 20% of the seafloor pressure. The two pistons are located at the forefront of the two chambers and the part of the sample chamber between the two pistons is filled with deionized water.

Status II: During the collection of a sample, the fluid enters the sampling cylinder and pushes the piston back forward. The deionized water enters the accumulator chamber through the orifice, thereby pushing the piston of the accumulator chamber to move backward. The two pistons keep moving until the internal pressure of the cylinder is balanced with the pressure of the outside seawater.

Status III: The high-pressure fluid inside the sampling cylinder will cause the expansion of the cylinder when the sampler is retrieved back to the deck. During this process, the compressed nitrogen gas compensates the pressure changes inside the cylinder.

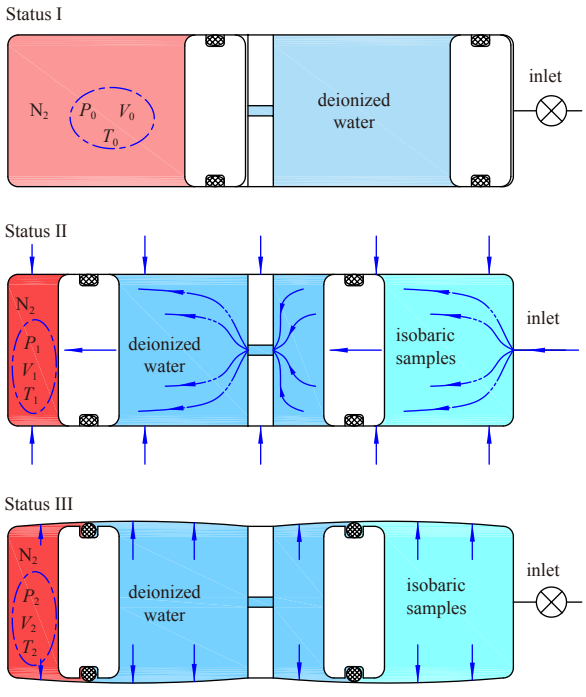

Fig. 5. Three sampling cylinder statuses.

4.2 *Calculation of pressure compensation effect*

According to the proposed real gas state equation, the parameters of gas in the three statuses have the following relationships:

$$\frac{P_0V_0}{T_0Z_0} = \frac{P_1V_1}{T_1Z_1} = \frac{P_2V_2}{T_2Z_2}, \tag{4}$$

where P, V, T and Z represent the pressure, volume, temperature and compression factor of the gas, respectively. The subscripts 0, 1 and 2 correspond to the three statuses described above.

The outside pressure of the cylinder is reduced to the atmospheric pressure after the sampler is retrieved on the deck. The cylinder produces an elastic volume expansion under the action of the internal pressure generated by the sample, compressed deionized water and gas. The theoretical volume change of the cylinder can be obtained by calculating the radial and axial deformations of the cylinder under the difference of the internal and external pressure. From this elastic theory, the radial deformation of the cylinder is shown as follows:

$$u = \frac{D_1^2P_i}{rE\left(D_2^2 - D_1^2\right)}\left[r^2\left(1-2\mu\right) + D_2^2\left(1+\mu\right)\right], \tag{5}$$

where P_i is the pressure of the samples, D_1 is the inner diameter of the cylinder, D_2 is the outer diameter of the cylinder, L is the length of the cylinder, r is the radius of the inner wall of the cylinder, E is the elastic modulus of material and μ is the Poisson ratios of the material.

The axial displacement of the cylinder is shown as follows:

$$\Delta L = \frac{D_1^2LP_i(1-2\mu)}{E(D_2^2 - D_1^2)}. \tag{6}$$

The volume change of the cylinder is then obtained:

$$\Delta V = \pi(D_1+u)^2\left(L+\Delta L\right)/4 - \pi D_1^2L/4. \tag{7}$$

Regardless of the volume change of the fluid sample and deionized water, the volume expansion of the sampling cylinder is compensated by the compressed gas. Hence, we can obtain the volume of the gas at Status III as follows:

$$V_2 = V_1 + \Delta V. \tag{8}$$

According to Eqs (1) and (4), the gas volume in Status II can be solved:

$$V_1 = \frac{P_0 V_0 T_1}{P_1 T_0} \cdot \frac{Z(P_1)}{Z(P_0)}. \tag{9}$$

Combining Eqs (4)–(9), we obtain:

$$\frac{P_2}{Z(P_2)} = \frac{P_0 V_0 T_2}{Z(P_0)\, T_0 (V_1 + \Delta V)}. \tag{10}$$

Since the ambient temperatures prior to deployment and after recovery of the sampler are equal, $T_0 = T_2$. From Eqs (9) and (10), we obtain:

$$\frac{P_2}{Z(P_2)} = \frac{1}{m}, \tag{11}$$

where

$$m = \frac{T_1 Z(P_1)}{P_1 T_0} + \frac{Z(P_0)\,\Delta V}{P_0 V_0}. \tag{12}$$

Combining Eqs (1) and (11), we obtain the solution for P_2 as follows:

$$P_2 = 353\ 03 \left[m - \sqrt{(0.008\ 619\ 4 - m)^2 - 4.559\ 9 \times 10^{-5}} \right] - 304.29. \tag{13}$$

Equation (13) provides a direct relationship of values between the maintained sample pressure and the precharged gas pressure. It can also provide theoretical guidance for the design parameters such as the length and radius of the sampling cylinder. In the actual operation, factors such as the changes in ambient temperature and the error of measurement will cause small deviations in the real effects of the pressure compensation.

The precharged gas pressure is usually set to 10% to 20% of the depth of the seabed when the sampler is deployed. The sample pressures of the sampler at different depths are calculated by introducing different precharged pressure values into Eq. (13). As shown in Fig. 6, it can be concluded that the sample pressure holding effect is better with an increased precharged gas pressure, which means that it has a strong ability to compensate for the decrease in pressure of a fluid sample. In addition, the separation distance of the several curves decreases with increasing precharged pressure at a high pressure range, which indicates that the maintenance effect of the sampler will not increase significantly with increasing precharged pressure. This also means that it is useless to blindly increase the precharged pressure in order to improve the maintenance effect of the pressure.

4.3 *Calculation of the sample volume*

The pressure of the precharged gas also has an effect on the sample volume. Since the total volume of the sampling cylinder is constant, the more gas that is precharged, the less sample will be collected. We designate the parameters of the sampling cylinder as follows: D is the internal diameter of the cylinder, L_s is the internal length of the sample chamber, L_g is the internal length of the accumulator chamber, and V_t is the total volume of the sampling cylinder. We have:

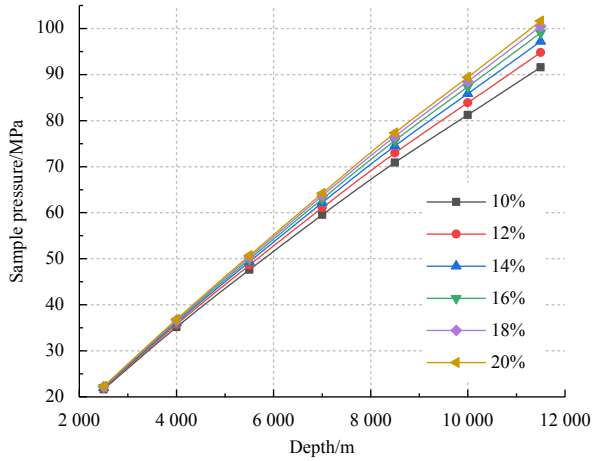

Fig. 6. The sample pressure curves of relationships between different precharged gas pressures and sampling depths.

$$V_t = \frac{\pi D^2 (L_g + L_s)}{4}. \tag{14}$$

After sampling, the pressures of the gas, sample and deionized water inside the sampling cylinder are equal. We assume that the compressed sample volume is V_{SC} and the compressed deionized water volume is V_{DC}. Since there is no change in the overall volume of the sampling cylinder before and after sampling, we can derive the following equation:

$$V_t = V_{SC} + V_{DC} + V_2. \tag{15}$$

At this time, the total volume of the compressed sample and the deionized water are equal to the sum of the volumes of the sample (V_s) and deionized water (V_d) at normal pressure and the total of the compressed fluid volume.

$$V_{SC} + V_{DC} = V_s + V_d + \frac{(V_{SC} + V_{DC}) \cdot P_2}{E_W}, \tag{16}$$

where E_W is the elasticity modulus of the deionized water.

The gas volume in the final state is shown as Eq. (17):

$$V_2 = \frac{P_0 V_0 T_2}{P_2 T_0} \cdot \frac{Z(P_2)}{Z(P_0)}. \tag{17}$$

Since the parameters in Eq. (4) are all known, the value of V_2 can be solved. According to Eqs (14)–(17), the sample volume V_s collected by the sampler is:

$$V_s = \frac{\pi D^2 \left[(E_W - P_2) L_g + P_2 L_S \right]}{4 E_W} + \frac{\pi D^2 L_g P_0 T_2 (P_2 - E_W)}{4 E_W P_2 T_0} \cdot \frac{Z(P_2)}{Z(P_0)}. \tag{18}$$

The data from different depths and different precharged gas pressures are brought into Eq. (18), and the corresponding sample volume is obtained, as shown in Fig. 7. The volume of the

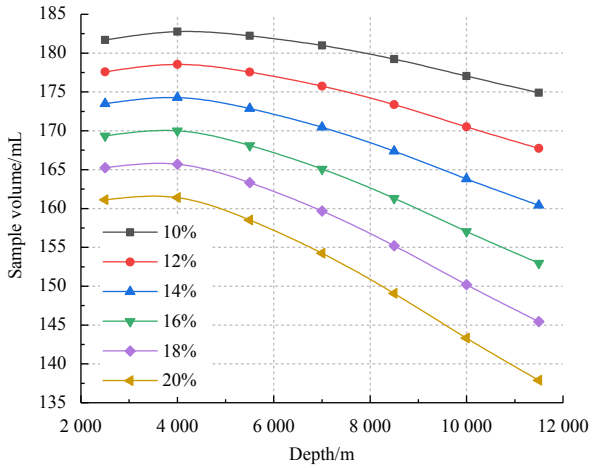

Fig. 7. The sample volume curves of relationships between different precharged gas pressures and sampling depths.

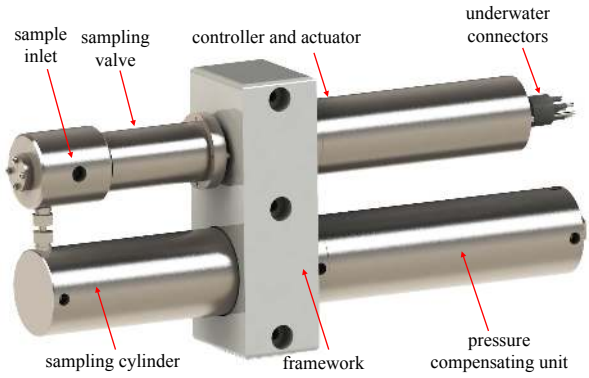

Fig. 8. Schematic diagram of the deep-sea pressure-maintaining sampler.

Fig. 9. Water sampling experiment of the samplers in the high-pressure vessel.

sample decreases with increasing sampler depth. Additionally, the volume of the sample at the same depth decreases with increasing precharged pressure.

5 Results and discussion

A high-pressure vessel experiment of a deep-sea pressure-maintaining sampler was conducted to verify the accuracy of the theoretical calculation method. The sampler mainly consisted of a sampling cylinder, a sampling valve and an actuator, which has the typical structure as has been reported previously (Fig. 8) (Wu et al., 2018). Six sets of these samplers were put into a high-pressure vessel for conducting water sampling (Fig. 9). The sampling pressure of the experiment was set to 115 MPa for simulating the full ocean depth environment.

After the initial and the final parameters of P, V and T of the experiment were recorded, the theoretical sample volume and pressure were calculated by using the equations in Section 4. As shown in Tables 3 and 4, the results of the calculations are very close to the practical values, which prove the precision of this calculation method. Compared to the ideal gas state equation, the calculation method presented in Section 4 provides a better calculation of the pressure and volume of the sampler sample.

For the sampler, we need to explore an appropriate usage rule to better meet the needs of scientific investigations. The sample volume and pressure of the sampler operating at 115 MPa pressure are calculated by setting different precharged pressures, as shown in Fig. 10. As the precharged pressure increases, the sample volume gradually decreases and the pressure of the sample increases. To better meet the requirements of the sample, scientists generally require that the pressure of the sample be closer to the in situ pressure. However, it is difficult for the sampler to ensure the in situ pressure. The better the pressure holding effect of the sampler is, the smaller the sample volume

Table 3. Sample pressure data from the simulation experiment

No.	Precharged pressure/MPa	Measured sample pressure/MPa	Calculated pressure/MPa	Relative error of calculated pressure/%	Calculated pressure using ideal EOS/MPa	Relative error using ideal EOS/%
1	23.5	102.9	102.54	0.3	55.93	45.6
2	23.5	102.4	102.23	0.2	55.93	45.4
3	23.2	103.1	102.61	0.5	55.78	45.9
4	18.4	102.1	100.89	1.1	53.60	47.5
5	19.3	102.7	101.51	1.1	53.99	47.4
6	19.3	102.7	101.51	1.1	53.99	47.4
7	19.3	103.2	101.86	1.3	53.99	47.7
8	19.0	102.5	101.35	1.2	53.86	47.5
9	18.6	100.3	99.90	0.4	53.69	46.5
10	19.0	100.1	99.84	0.2	53.86	46.2
11	18.6	98.6	98.84	0.3	53.69	45.5
12	18.9	95.1	96.76	1.8	53.82	43.4
13	18.9	100.2	99.89	0.3	53.82	46.3

Table 4. Sample volume data from the simulation experiment

No.	Precharged pressure/MPa	Measured sample volume/mL	Calculated volume/mL	Relative error of calculated volume/%	Calculated volume using ideal EOS/mL	Relative error using ideal EOS/%
1	23.5	135.8	136.70	0.7	170.80	25.8
2	23.5	136.7	136.47	0.2	170.49	24.7
3	23.2	136.8	137.83	0.8	171.53	25.4
4	18.4	156.0	154.12	1.2	180.70	15.8
5	19.3	152.1	151.23	0.6	179.20	17.8
6	19.3	149.3	151.22	1.3	179.20	20.0
7	19.3	155.6	151.45	2.6	179.52	15.4
8	19.0	151.2	152.22	0.7	179.74	18.9
9	18.6	153.4	152.75	0.4	179.35	16.9
10	19.0	149.9	151.24	0.9	178.36	19.0
11	18.6	151.2	152.08	0.6	178.38	18.0
12	18.9	150.4	149.61	0.5	175.67	16.8
13	18.9	152.8	151.64	0.8	178.64	16.9

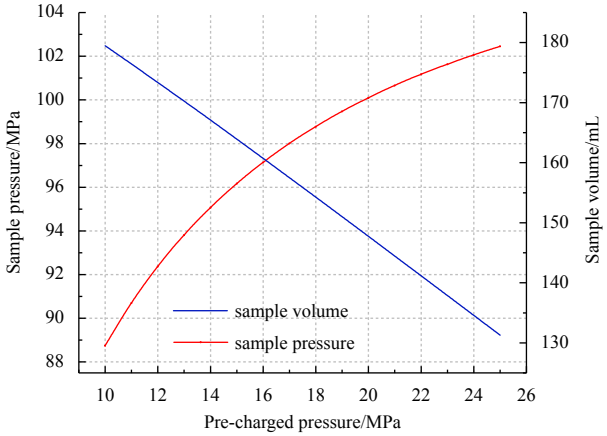

Fig. 10. The sample pressure and sample volume on different precharged gas pressures when operating at 115 MPa.

obtained. During actual applications, the pressure value of precharged gas is usually set to be 10%~20% of the bottom pressure. This requires the users to set an appropriate precharged pressure for the gas according to the actual needs of the scientific investigation.

6 Conclusions

The calculation errors of the existing gas state equations increase as the pressure increases over 30 MPa. We proposed an empirical gas state equation based on the compression factor Z which was obtained by quadratic polynomial regression of the experimental data. It shows adequate accuracy for compressed nitrogen gas with a pressure ranging from 15 to 120 MPa. Furthermore, the theoretical calculations of the pressure and volume of the deep-sea sampler combined with the proposed gas state equation were described in detail. Water sampling experiments inside the high-pressure vessel were constructed, and the results demonstrated the accuracy of the theoretical calculation method. The theory of pressure compensation can provide theoretical guidance not only for the design and operation of deep-sea samplers but also for other high-pressure instruments associated with compressed gases.

Acknowledgements

We thank Bo Zhang and Xun Wang for previous laboratory experiment. We also thank Guorui Zhong and Zhiwei Zhu for their support in the high-pressure vessel experiments.

References

Bianchi A L, Garcin J, Tholosan O. 1999. A high-pressure serial sampler to measure microbial activity in the deep sea. Deep Sea Research Part I: Oceanographic Research Papers, 46(12): 2129–2142, doi: 10.1016/S0967-0637(99)00039-4

Drazen J C, Bird L E, Barry J P. 2005. Development of a hyperbaric trap-respirometer for the capture and maintenance of live deep-sea organisms. Limnology and Oceanography: Methods, 3(11): 488–498, doi: 10.4319/lom.2005.3.488

Drazen J C, Yeh J. 2012. Respiration of four species of deep-sea demersal fishes measured in situ in the eastern North Pacific. Deep Sea Research Part I: Oceanographic Research Papers, 60: 1–6, doi: 10.1016/j.dsr.2011.09.007

Halder G. 2014. Introduction to Chemical Engineering Thermodynamics. 2nd ed. New Delhi: PHI Learning Private Limited, 45–63

Hempert F, Boblest S, Ertl T, et al. 2017. Simulation of real gas effects in supersonic methane jets using a tabulated equation of state with a discontinuous Galerkin spectral element method. Computers & Fluids, 145: 167–179

Huang Haocai, Huang Liang, Ye Wei, et al. 2018. Optimizing preloading pressure of precharged gas for isobaric gas-tight hydrothermal samplers. Journal of Pressure Vessel Technology, 140(2): 021201, doi: 10.1115/1.4038901

Huang Zhonghua, Liu Shaojun, Jin Bo. 2006. Accumulator-based deep-sea microbe gastight sampling technique. China Ocean Engineering, 20(2): 335–342

Jannasch H W, Wirsen C O. 1977. Retrieval of concentrated and undecompressed microbial populations from the deep sea. Applied and Environmental Microbiology, 33(3): 642–646, doi: 10.1128/AEM.33.3.642-646.1977

Kim S J, Kato C. 2010. Sampling, isolation, cultivation, and characterization of piezophilic microbes. In: Timmis K N, ed. Handbook of Hydrocarbon and Lipid Microbiology. Berlin Heidelberg: Springer-Verlag, 3869–3881

Koyama S, Miwa T, Horii M, et al. 2002. Pressure-stat aquarium system designed for capturing and maintaining deep-sea organisms. Deep Sea Research Part I: Oceanographic Research Papers, 49(11): 2095–2102, doi: 10.1016/S0967-0637(02)00098-5

Martin J J, Hou Yuchun. 1955. Development of an equation of state for gases. AIChE Journal, 1(2): 142–151, doi: 10.1002/aic.690010203

McNichol J, Sylva S P, Thomas F, et al. 2016. Assessing microbial processes in deep-sea hydrothermal systems by incubation at *in situ* temperature and pressure. Deep Sea Research Part I: Oceanographic Research Papers, 115: 221–232, doi: 10.1016/j.dsr.2016.06.011

Monago K O. 2010. Equation of state for gaseous nitrogen determ-

ined from isotropic model potentials. The Canadian Journal of Chemical Engineering, 88: 55–62, doi: 10.1002/cjce.20257

Pavithran S, Ingole B, Nanajkar M, et al. 2007. Macrofaunal diversity in the Central Indian Ocean Basin. Biodiversity, 8(3): 11–16, doi: 10.1080/14888386.2007.9712824

Peng Dingyu, Robinson D B. 1976. A new two-constant equation of state. Industrial & Engineering Chemistry Fundamentals, 15(1): 59–64

Peoples L M, Norenberg M, Price D, et al. 2019. A full-ocean-depth rated modular lander and pressure-retaining sampler capable of collecting hadal-endemic microbes under *in situ* conditions. Deep Sea Research Part I: Oceanographic Research Papers, 143: 50–57, doi: 10.1016/j.dsr.2018.11.010

Priede I G. 2018. Buoyancy of gas-filled bladders at great depth. Deep Sea Research Part I: Oceanographic Research Papers, 132: 1–5, doi: 10.1016/j.dsr.2018.01.004

Redlich O, Kwong J N S. 1949. On the thermodynamics of solutions. V. An equation of state. Fugacities of gaseous solutions. Chemical Reviews, 44(1): 233–244

Rossel P E, Stubbins A, Rebling T, et al. 2017. Thermally altered marine dissolved organic matter in hydrothermal fluids. Organic Geochemistry, 110: 73–86, doi: 10.1016/j.orggeochem.2017.05.003

Shillito B, Ravaux J, Sarrazin J, et al. 2015. Long-term maintenance and public exhibition of deep-sea hydrothermal fauna: the AbyssBox project. Deep Sea Research Part II: Topical Studies in Oceanography, 121: 137–145, doi: 10.1016/j.dsr2.2015.05.002

Smith J M, van Ness H C, Abbott M M. 2005. Introduction to Chemical Engineering Thermodynamics. 7th ed. New York: McGraw-Hill, 35–46

Soave G. 1972. Equilibrium constants from a modified Redlich-Kwong equation of state. Chemical Engineering Science, 27(6): 1197–1203, doi: 10.1016/0009-2509(72)80096-4

Wu Tao, Tao Chunhui, Zhang Jinhui, et al. 2019. A hydrothermal investigation system for the *Qianlong-II* autonomous underwater vehicle. Acta Oceanologica Sinica, 38(3): 159–165, doi: 10.1007/s13131-019-1408-4

Wu Shijun, Wang Shuo, Yang Canjun. 2018. Collection of gas-tight water samples from the bottom of the challenger deep. Journal of Atmospheric and Oceanic Technology, 35(4): 837–844, doi: 10.1175/JTECH-D-17-0170.1

Wu Shijun, Yang Canjun, Chen Ying, et al. 2010. A study of the sealing performance of a new high-pressure cone valve for deep-sea gas-tight water samplers. Journal of Pressure Vessel Technology, 132(4): 041601, doi: 10.1115/1.4001204

Yamamoto K. 2015. Overview and introduction: Pressure core-sampling and analyses in the 2012–2013 MH21 offshore test of gas production from methane hydrates in the eastern Nankai Trough. Marine and Petroleum Geology, 66: 296–309, doi: 10.1016/j.marpetgeo.2015.02.024

Zhang Zenghu, Wu Yanhong, Zhang Xiaohua. 2018. Cultivation of microbes from the deep-sea environments. Deep Sea Research Part II: Topical Studies in Oceanography, 155: 34–43, doi: 10.1016/j.dsr2.2017.07.008